Analysis of the low-pressure low-current dc positive column in neon

Edward A. Richley*
P.O. Box 64, Gaithersburg, Maryland 20884-0064

(Received 15 December 2001; revised manuscript received 7 March 2002; published 7 August 2002)

A time-dependent, nonstatistical analysis of the positive column in low-pressure neon is presented. The analysis is based on the elliptic representation of the Boltzmann equation and so is tolerant of large degrees of anisotropy. A self-consistent absorbing wall boundary condition is described, along with a time-dependent form of Poisson's equation. The equations are cast in a form that lends itself to a numerical implementation based on a well established low phase-error monotonic method. An instability with short time scale is predicted near the wall, and is analyzed. A scaling law for the various anisotropic components in the nonlocal regime is derived, and a critical analysis of the nonlocal electron kinetic method is presented.

DOI: 10.1103/PhysRevE.66.026402 PACS number(s): 52.80.Hc, 52.65.−y, 52.27.−h

I. INTRODUCTION

Despite its long history, the low-pressure positive column continues to be the subject of much theoretical analysis [1–5]. Owing to the increasing availability of computational power, and to the inapplicability of various simplifying assumptions under low-pressure and low-current conditions, these models have become increasingly sophisticated.

The concern of these more recent models is that at sufficiently low pressures and low currents, the electron velocity distribution function (EVDF) is not accurately described by a singly parametrized function, be it Maxwellian or otherwise. Rather, it must be determined with both energy and space resolution. For any reasonable accuracy, a solution requires a significant amount of computation. Furthermore, the relevant time scales involved range from the time required for the fastest electrons in the simulation to cross a computational cell (of the order of 1 ps) to the time scale for thermal relaxation of the neutral host gas (typically 100 μs). This disparity makes the system quite stiff and, hence, computationally challenging.

At the highest energies of interest, and at absorbing boundaries, the distribution function will exhibit high angular anisotropy. This anisotropy can be so great as to render the two-term spherical harmonic expansion invalid in those regions. As it is impossible to determine *a priori* which regions of phase space will be in violation without risking a compromised solution, a robust representation of the Boltzmann equation is needed in order to smoothly transit to higher degrees of anisotropy when and where they occur.

The primary purpose of the present work is to cast the Boltzmann equation, and other transport equations needed for a description of the positive column, in such a manner that a robust, self-consistent solution can be obtained by the use of a well-established time-dependent numerical technique of known accuracy and stability. The particularly novel features of the present work are: (1) an implementation of the elliptic representation of the Boltzmann equation as it applies to the positive column [6]; (2) a time-dependent solution, resolved in energy, utilizing a monotonic method; (3) an absorbing-wall boundary condition that has validity for all degrees of anisotropy; (4) a time-dependent representation of Poisson's equation, which is well suited for monotonic methods; and (5) inclusion of the effects of neutral gas heating.

II. BACKGROUND

Although the positive column of the low-pressure glow discharge has been observed experimentally for over 140 years [7–9] its theoretical investigation has lagged somewhat behind experiment and commercial application. The first published model of any significance was by Schottky [10] in 1924, followed thereafter by the more general treatment by Tonks and Langmuir [11]. Various refinements of this class of model followed [12–14], yet all relied on the assumption that electrons exhibit a Maxwellian distribution, with a radially uniform temperature. Furthermore, the relation between electron temperature and ionization rate was left unspecified, and the radial transport of electron energy was not included.

Radial flow of electron energy was eventually found to be a necessary component of models, especially at lower pressure. A nice presentation of the evolution of these ideas is given by Ingold [15]. Notwithstanding these refinements, these models rely on a fluid or moment description of electrons, in which they are assumed to have a known, though possibly parametrized, distribution function.

As an intermediate step between such moment models and an energy-resolved Boltzmann solution, the nonlocal electron kinetic (NEK) approach [5,16–18] has recently been applied to the positive column. However, as the following analysis shows, there is some reason to doubt the validity of this method.

The NEK method is considered to be applicable when tube radius R is much smaller than the energy relaxation distance for elastic collisions, λ_T. The isotropic component of the distribution function, f_0, is expanded as follows:

$$f_0(\varepsilon,\varrho)=f_0^0(\varepsilon)+f_0^1(\varrho,\varepsilon)+f_0^2(\varrho,\varepsilon)+f_0^3(\varrho,\varepsilon)+\cdots, \tag{1}$$

where ϱ is the dimensionless radial position coordinate and ε is the dimensionless ''total'' energy coordinate. According

*Email address: richley@mailaps.org

to the procedure, spatial averaging is used to obtain f_0^0, and each successive term is obtained by a perturbation method.

In order to analyze the validity of this method, a simple case will be considered. In this case, cylindrical geometry is chosen, and the radial potential is assumed to have a parabolic profile. Only those electrons that are ''trapped'' with energy less than the wall potential will be treated, and ionization is ignored in this example. A constant mean free path for elastic collisions is assumed. These conditions yield a particularly simple form of the Boltzmann equation, and a particularly simple form for each of the terms in the expansion. Details are provided elsewhere [19], with the result that each term can be represented as a product of a polynomial, $p_n(\varrho,\varepsilon)$, and an exponential:

$$f_0^n = \beta^n p_n(\varrho,\varepsilon) e^{-\varepsilon^2}, \tag{2}$$

where β is a dimensionless ratio, presumed to be much smaller than unity, defined by

$$\beta = \frac{E_z \lambda_T}{4\tilde{\phi}_w}\left(\frac{R}{\lambda_T}\right)^2, \tag{3}$$

where E_z is the axial field and $\tilde{\phi}_w$ is the wall potential. It is the factor of β^n which is presumed to cause convergence of the series. However, it is necessary to consider the magnitude of p_n, with the polynomial given by

$$p_n(\varrho,\varepsilon) = \sum_{i,j}^{n} a_{ij}^n \varrho^i \varepsilon^j + \sum_{i=0}^{n} b_i \varepsilon^i. \tag{4}$$

A recursion relation is obtained for the coefficients of p_{n+1} in terms of those of p_n. Beginning with $p_0 = 1$, the remaining polynomials have been determined by the use of a computer program [20]. The magnitude of the largest coefficient $|a_{ij}^n|$ of each polynomial is found to grow *faster than exponentially* with *n*. The exponential factor β^n is thus overwhelmed by the polynomial p_n as *n* increases. As a consequence, the series cannot be considered to be convergent, and the entire method must be considered to be of questionable validity.

More recently, energy-resolved solutions have been developed. Some are based on statistical representations of the underlying kinetics using quasiparticle techniques, such as Monte Carlo [1,21]. These are useful, but suffer from the usual limitations of statistical approaches in that the number of particles that must be simulated becomes prohibitive as more of the ''tail'' of the EVDF is included.

Other kinetic-based schemes have been devised, which treat the EVDF by a sequence of convective steps and collision steps [2,22] in which the convective steps are treated with very high accuracy. However, remapping onto the grid is required and the amount of error introduced by this process is difficult to quantify. Furthermore, this is also true for quasiparticle schemes, not all quantities in the simulation are appropriately treated by this process, leading to a hybrid scheme in order to obtain a self-consistent solution.

Eulerian continuum approaches avoid these difficulties. These are often based on the two-term spherical harmonic expansion [3,4] in steady state form. These tend to describe the EVDF well, but have difficulty in regions where anisotropy is large and where the two-term expansion is, therefore, invalid. However, the choice of a particular closure to that expansion forms the elliptic representation [6] that does not suffer from such a limited range of validity. Furthermore, dynamic effects can be included by seeking a time-dependent solution to the Boltzmann equation. The elliptic representation, in time-dependent form, is the basis for the present work.

The time-dependent elliptic representation fits into the general form of time-dependent transport equations, for which numerical solution techniques are well established [23]. Although such equations are generally used in the treatment of reactive flow [24], their computational domain is easily extended to include both space and energy dimensions as is needed for the energy-resolved description of electrons. The heavy particles (ions and neutral gas) are treated as fluids in the conventional sense (space only). The components of the electric field can also be represented in this form. Thus, one uniform solution technique can be used to describe the evolution of all quantities.

A method based on flux-corrected transport (FCT) [23] is used for the solution, with the multidimensional extension of Zalesak [25] providing the framework for the quantities defined on phase space. Convection terms are evaluated using FCT, while the ''source'' terms representing body forces, pressure gradients, collisions, etc. are included with fractional-step coupling. Provisions are made for second-order time accuracy with a Runge-Kutta style time stepping for the convection steps, while all source terms are subjected to Richardson extrapolation [26]. Since this is a time-dependent simulation, the computation progresses until some prechosen total simulation time has been reached.

There are several advantages of this approach. Short-wavelength numerical phenomena are substantially suppressed by the monotonic convection algorithm, while the numerical dissipation for longer wavelengths is substantially removed. These considerations are particularly important for such a problem in which conditions vary widely across configuration and energy space. Very little *a priori* knowledge about flow regime (convective vs diffusive, supersonic vs subsonic) or strong nonlinearities (steep gradients) is needed in order to obtain a stable and accurate solution. Furthermore, no assumptions about the dynamic stability of the system of equations need be made, and no selection rules for various possible branches (regarding, for example, the sonic singularity of ion transport [27]) in the solution need be devised.

III. ELECTRON EQUATIONS

As pointed out in Ref. [6], the elliptic representation can be viewed as a particular closure to the two-term spherical harmonic expansion. However, rather than the traditional components $f_0(r,u)$ (isotropic) and $\vec{f}_1(r,u)$ (anisotropic), it

is advantageous to define new quantities, and to choose the dependent variables as

$$\eta(r,u)=v n(r,u)=4\pi v f_0(r,u) \tag{5}$$

and

$$\vec{X}(r,u)=\frac{\vec{\Gamma}(r,u)}{n(r,u)}=\frac{1}{3}\frac{\vec{f}_1(r,u)}{f_0(r,u)}, \tag{6}$$

where v is the electron speed $[u=(m/2e)v^2]$, and $n(r,u)$ and $\vec{\Gamma}(r,u)$ are the original variables defined in Ref. [6]. This new choice of variables ensures that derived quantities will be the result of *multiplication* of monotonic quantities, and not division. This process tends to suppress short-wavelength (grid-sized) phenomena without the need to include artificial dissipation [28].

The equations of the elliptic representation can be rewritten for cylindrical geometry and axial uniformity as

$$\frac{\partial\eta}{\partial t}+\frac{1}{r}\frac{\partial(r\eta v\vec{X})}{\partial r}-\frac{\partial}{\partial u}[v(\vec{E}\cdot\vec{X}\eta)]=\left(\frac{\delta\eta}{\delta t}\right)_{coll} \tag{7}$$

and

$$\begin{aligned}
&\frac{\partial\vec{X}}{\partial t}+vX_r\frac{\partial\vec{X}}{\partial r}-v(\vec{E}\cdot\vec{X})\frac{\partial\vec{X}}{\partial u}+\frac{1}{r}\frac{\partial}{\partial r}\left\{rv\left[\frac{1}{2X^2}\left(3\frac{X}{\gamma}-1\right)-1\right]X_r\vec{X}\right\}-\frac{\partial}{\partial u}\left\{v\left[\frac{1}{2X^2}\left(3\frac{X}{\gamma}-1\right)-1\right](\vec{E}\cdot\vec{X})\vec{X}\right\}\\
&=-\vec{X}vX_r\left[\frac{1}{2X^2}\left(3\frac{X}{\gamma}-1\right)-1\right]\frac{1}{\eta}\frac{\partial\eta}{\partial r}+\vec{X}\left[\frac{1}{2X^2}\left(3\frac{X}{\gamma}-1\right)-1\right]v(\vec{E}\cdot\vec{X})\frac{1}{\eta}\frac{\partial\eta}{\partial u}-\left\{\frac{\partial}{\partial r}\left[\frac{v}{2}\left(1-\frac{X}{\gamma}\right)\right]+\frac{v}{2}\left(1-\frac{X}{\gamma}\right)\frac{1}{\eta}\frac{\partial\eta}{\partial r}\right\}\hat{\boldsymbol{r}}\\
&+\left\{v\frac{\partial}{\partial u}\left[\frac{1}{2}\left(1-\frac{X}{\gamma}\right)\right]+v\frac{1}{2}\left(1-\frac{X}{\gamma}\right)\frac{1}{n}\frac{\partial n}{\partial u}\right\}\vec{E}+\frac{1}{2X^2}\left(3\frac{X}{\gamma}-1\right)\frac{v}{2u}[\vec{X}(\vec{E}\cdot\vec{X})-X^2\vec{E}]+\left(\frac{\delta\vec{X}}{\delta t}\right)_{coll},
\end{aligned} \tag{8}$$

where $\vec{E}$ is the electric field, $X=|\vec{X}|$, the eccentricity, $\gamma=\gamma(X)$, is defined in Ref. [6], and $n=\eta/v$ from Eq. (5).

The collision operators $(\delta(\cdot)/\delta t)_{coll}$ consist of contributions from elastic collisions with neon atoms, inelastic excitation collisions with neon for the excited states 3S3P1, 3S1P1, 3S3P2, 3S3P0, and a lumped 3P state, and ionization collisions for neon in the ground state as well as in the 3S3P2 and 3S3P0 metastable states. These terms follow the forms outlined in Ref. [6].

Kinetic data for elastic collisions are taken from Robertson [29], Massey and Burhop [30], and Register and Trajmar [31]. Data for the inelastic collision terms for excitation are taken from Register *et al.* [32].

Ionization collisions are treated with the assumption of equal energy sharing of the newly created electron with the scattered electron [33], which is a suitable approximation for the low energies expected in the positive column. Each of these collisions have a different target species, since ionization from metastables is allowed. This term is represented as

$$\left(\frac{\delta\eta}{\delta t}\right)_{ion}=\sum_i N_j(r)[4\eta'\sigma_{i,T,j}(v')v'-\eta\sigma_{i,T,j}(v)v], \tag{9}$$

where v' is defined in terms of the v and the ionization energy u_i by $\frac{1}{2}mv'^2=mv^2+u_i$, and $N_j(r)$ is the concentration of the target species. Kinetic data are taken from Johnston *et al.* [34] and Rapp and Englander-Golden [35].

The left hand side of Eq. (8) includes both convection *and* advection operators. On the right are various terms proportional to the logarithmic derivatives of η or n. The second to last term on the right hand side is a "rotation" term that serves not to change the magnitude of $\vec{X}$ (as can be seen from formation of its dot product with $\vec{X}$), but only to rotate $\vec{X}$ toward the negative of the direction of $\vec{E}$.

Considering each term separately, it can be seen that all terms aside from the advection terms, the rotation term, and the collision term actually disappear as $|\vec{X}|\to 1$. The rotation term does not change the magnitude of $\vec{X}$, while the advection terms serve only to move the $\vec{X}$ field around in phase space, and can create no new maxima or minima. Thus, as long as the collision term is well behaved, Eq. (8) has the proper asymptotic behavior in that the anisotropy is limited in its growth to physically reasonable values $(|\vec{X}|<1)$.

The collision term is, from the definition of $\vec{X}$,

$$\left(\frac{\delta\vec{X}}{\delta t}\right)_{coll}=\frac{v}{\eta}\left(\frac{\delta\vec{\Gamma}}{\delta t}\right)_{coll}-\vec{X}\frac{1}{\eta}\left(\frac{\delta\eta}{\delta t}\right)_{coll}. \tag{10}$$

Following the approximations of Ref. [6], the first term is

$$\begin{aligned}
\frac{v}{\eta}\left(\frac{\delta\vec{\Gamma}}{\delta t}\right)_{coll}\approx-\Bigg(&N(r)\sigma_{el,M}(v)+N(r)\sum_j\sigma_{ex,M,j}(v)\\
&+\sum_j N_j(r)\sigma_{i,M,j}(v)\Bigg)v\vec{X},
\end{aligned} \tag{11}$$

where $\sigma_{ex,M,j}()$ denotes the momentum transfer cross section for the excitation process denoted by j. The second term follows from the previously computed term, $(\delta\eta/\delta t)_{coll}$.

It is interesting to take the terms of Eq. (10) back to their definitions in Sec. IV of Ref. [6], and to note that the outscattering terms identically cancel, leaving only the inscattering terms. Thus, the strict definitions of the collision terms lead from Eq. (10) directly to

$$\left(\frac{\delta\vec{X}}{\delta t}\right)_{coll} = N(r)v\frac{\eta(v')}{\eta(v)}\left(\frac{v'^4}{v^4}\right)[\sigma_{el,P}(v')\vec{X}(v') - \sigma_{el,T}(v')\vec{X}(v)] + N(r)v\frac{\eta(v')}{\eta(v)}\sum_j\left(\frac{v'^2}{v^2}\right) \times[\sigma_{ex,P,j}(v')\vec{X}(v') - \sigma_{ex,T,j}(v')\vec{X}(v)] + v\frac{\eta(v')}{\eta(v)}\sum_j N_j(r)\left(\frac{v'^2}{v^2}\right)[\sigma_{i,P,j}(v')\vec{X}(v') - \sigma_{i,T,j}(v')\vec{X}(v)]. \quad (12)$$

From their definitions, $\sigma_P(v)<\sigma_T(v)$ for all collisions, so that as $|\vec{X}|\to 1$, each negative term will always be greater than the corresponding positive term, as long as $|\vec{X}(v')|$ is also limited. However, $|\vec{X}(v')|$ is also limited by a similar process, so that as long as proper asymptotic behavior is provided at the boundaries, it will be preserved everywhere. Thus, and as one would expect, collisions limit the growth of anisotropy, and generally contribute to its reduction.

The boundary conditions must be established for η and $\vec{X}$ at $u=0$, $u=u_{max}$, $r=0$, and $r=R$. Within the finite-difference context, these are described by the inclusion of an extra layer of ''guard cells'' surrounding the computational domain. For the two-dimensional space (r,u), the computational domain $[i,j]$ is defined by $1<i<N$ and $1<j<M$. The boundary condition formulas must determine the contents of cells at $[0,j]$, $[N+1,j]$, $[i,0]$, and $[i,M+1]$ in terms of the values within the domain. The physical boundaries are then located at the midpoints between guard cells and their nearest neighbors within the boundaries.

Mathematically, not all of these conditions are needed for all components. However, *numerically*, the guard cell values are needed for proper operation of the flux-correction algorithm, which effectively makes all time-dependent equations second order in all space dimensions (albeit generally with vanishing second-order contributions).

At $u=0$ in the absence of any source of electrons there, it follows that $\vec{X}(r,0)=0$, and that $\vec{X}[i,0]=-\vec{X}[i,1]$. The condition for $\eta(r,0)$ can be obtained from the integration of Eq. (23) of Ref. [6] (after multiplying by v^3dv) between $v=0$ and some small value of v. Considering that $|\vec{\Gamma}|$ must be of order v in this region, and the nature of the quantity X/γ (which has no first-order dependence, as seen from Fig. 2 of Ref. [6]), it follows directly that $\partial n/\partial u|_{u=0}=0$. Thus, it would seem correct to set $\eta(r,0)=0$ with an apparent singularity in $\partial\eta/\partial u|_{u=0}$. However, it is also necessary to set all fluxes at this boundary to zero, including the diffusion/antidiffusion fluxes of FCT. In fact, it is only these fluxes that necessitate a condition on this boundary (all other flux terms vanish naturally at $u=0$). Since the domain is restricted to positive values of u, suppression of fluxes is accomplished by setting

$$\eta[i,0]=\eta[i,1], \quad (13)$$

and the resulting solution will enforce the limit of $\eta|_{u=0}\to 0$, as grid spacing Δu vanishes.

At $r=0$ a similar symmetry condition requires that $X_r(0,u)=0$, while $\partial\eta/\partial u|_{r=0}=0$. Thus

$$\eta[0,j]=\eta[1,j], \quad X_r[0,j]=-X_r[1,j]. \quad (14)$$

At $u=\infty$ the boundary conditions clearly require that $\eta\to 0$ and $\vec{\Gamma}\to 0$. However, the means for representing this limiting trend for some finite maximum value of $u=u_{max}$ has not been thoroughly examined in the literature. Simply taking $\eta[i,M+1]=0$ and $\vec{\Gamma}[i,M+1]=0$ tends to incorrectly estimate the flux across the boundary. Various attempts to create an outflow boundary condition that supports correct wave motion across the boundary have also been found to be inadequate. What seems to work best is a simple extrapolation of the tail of the distribution function onto the guard cell. The extrapolation can be implemented in various ways, but a simple method is to project logarithmically from some value of $u<u_{max}$, through u_{max}, and onto the guard cell. This projection is done for η and $v\vec{\Gamma}$ with the same factor, so that anisotropy, and hence $\vec{X}$, is unchanged across this boundary.

At $r=R$ there is an absorbing-wall boundary condition. This condition has received significant attention in the literature, and is especially critical for a continuum description that pays strict attention to correct asymptotic behavior with regard to anisotropy. For example, a similar problem considered by Morse and Feshbach [36] arrives at an approximate condition based on angular averaging resulting in a choice of $f_1\approx 1.5f_0$. This clearly violates the very assumption of low anisotropy upon which the condition is based.

Similarly, a ''loss-cone'' concept has been introduced [3,5] in which electrons in the final cell nearest to the absorbing wall are absorbed with a rate determined by the fraction of electrons with sufficient radial velocity to overcome the potential of an assumed infinitesimal sheath. In addition to requiring knowledge of this assumed potential, this model also depends upon an assumption of small anisotropy, without including the effects of anisotropy in the model itself. Thus, in conditions for which the wall absorption is significant enough to cause large distortions to the angular distribution, this model will not result in proper asymptotic behavior.

Still other analyses exist [4] for which a functional form for $f_{1r}(R,u)$ is assumed, without strict physical basis.

In the present work, a boundary condition has been devised, which allows for proper asymptotic behavior under all degrees of anisotropy, as well as for all ranges of grid spacing (Δr) and mean free path (λ_M). This condition is based

on the idea that the absorbing wall of the bound column is equivalent to an unbound domain containing an infinitesimally thin, perfectly absorbing sheet located at position $r=R$. This sheet has an infinite absorption rate for electrons that reach position $r=R$ and are moving with positive radial velocity. Thus, electrons at the wall are absorbed according to the rate term

$$\left(\frac{\delta f}{\delta t}\right)_W = \begin{cases} -v_r f v_r \delta(r-R) & \text{if } v_r > 0, \\ 0 & \text{if } v_r \leqslant 0, \end{cases} \tag{15}$$

where v_r is the radial component of velocity and the delta function $\delta()$ accomplishes the infinite absorption rate in an infinitesimal region. In the discrete space of the computational domain, subscript W indicates that the term applies in the last computational cells, $[N,j]$, near the wall, and the infinite rate is approximated with a rectangular function:

$$\left(\frac{\delta f}{\delta t}\right)_W \approx \begin{cases} -(v_r/d) f P(\vec{v}) & \text{if } v_r > 0, \\ 0 & \text{if } v_r \leqslant 0, \end{cases} \tag{16}$$

where $d=\frac{1}{2}\Delta r$ is half the grid spacing at the wall and $P(\vec{v})$ is a function necessary to take into account the fact that for a finite value of d, there is also a finite probability for collisions to occur with other species (that is, not *all* electrons within distance d of the wall having positive v_r will actually reach the wall; it is inherently a multibody collision).

$P(\vec{v})$ can undoubtedly take on many forms for purposes of approximation. It is only necessary that $P(\vec{v})\to 1$ as $\xi=\lambda_M/d\to\infty$, and $P(\vec{v})\to 0$ as $\xi\to 0$. One such approximation is the exponential relation

$$P(\vec{v}) = e^{-\xi(v/v_r)}. \tag{17}$$

This approximation also accounts for the particular direction of the electron and hence the fact that its distance to the wall along its path may be different from its perpendicular distance to the wall.

The angular moments of this collision term can now be taken according to the methods outlined in Ref. [6]. For the isotropic component of f, one obtains

$$\left(\frac{\delta \eta}{\delta t}\right)_W = -\frac{\gamma \eta(r,u)}{2\pi \ln\left(\frac{1+\gamma}{1-\gamma}\right)}\left(\frac{v}{d}\right) \times \int_0^{2\pi}\int_0^{\pi/2} \frac{\cos(\psi)\sin(\psi) e^{-(d/\lambda_M \cos(\psi))}}{1-\gamma_r\cos(\psi)-\gamma_z\sin(\psi)\cos(\phi)} d\psi\, d\phi, \tag{18}$$

where ψ is the angle in the *lab* frame to the radial outward direction and ϕ is the corresponding azimuthal angle. γ_r and γ_z are the radial and axial components of vector eccentricity, $\vec{\gamma}=(\gamma/X)\vec{X}$. Expressions similar to Eq. (18) for the anisotropic components follow in a similar manner [37].

From these integrals, two terms are obtained for each component of the distribution function. One is proportional to the same component, and the other is proportional to the radial component of $\vec{\Gamma}$. The first term acts as a collisional absorption term that is only active in the last cell near the wall. The other term has properties similar to a corresponding radial derivative term in the dynamic equation [Eqs. (7) and (8)] for each component, and can be combined with that term by forming an equivalent continuous projection onto the space beyond the wall. A complete derivation is provided elsewhere [37]. The result is that the absorbing-wall boundary condition can be represented by both an absorption term *and* a boundary condition. For the isotropic component η, the absorption term is

$$\left(\frac{\delta \eta}{\delta t}\right)_W = -E_3(\xi)\left(\frac{v}{d}\right) P_n(\vec{\gamma})\,\eta, \tag{19}$$

where

$$P_n(\vec{\gamma}) = \frac{1}{\gamma \ln\left(\frac{1+\gamma}{1-\gamma}\right)}\left\{ 2\left(1-\sqrt{1-\gamma_z^2}\right) + \frac{\gamma_r}{\gamma}\ln\left[\frac{(\gamma-\gamma_r)}{(\gamma+\gamma_r)}\frac{(\gamma\sqrt{1-\gamma_z^2}+\gamma_r)}{(\gamma\sqrt{1-\gamma_z^2}-\gamma_r)}\right]\right\}, \tag{20}$$

and similar expressions are derived for the anisotropic components.

The boundary condition is

$$\eta[N+1,j] = [4E_3(\xi)-1]\,\eta[N,j]. \tag{21}$$

Each of the components of $\vec{\Gamma}$ has a similar condition, so that $\vec{X}$ is unchanged across this boundary ($\vec{X}[N+1,j]=\vec{X}[N,j]$).

The absorption term for $\vec{X}$ is

$$\left(\frac{\delta \vec{X}}{\delta t}\right)_W = -E_3(\xi)\left(\frac{v}{d}\right)\{[P_n(\vec{\gamma})+P_r(\vec{\gamma})]X_r\hat{\boldsymbol{r}} + [P_n(\vec{\gamma})+P_z(\vec{\gamma})]X_z\hat{\boldsymbol{z}}\}, \tag{22}$$

where $P_r()$ and $P_z()$ are functions similar to $P_n()$ [37].

This boundary condition has proper asymptotic behavior for all degrees of anisotropy ($\gamma_r\to 0$, $\gamma_r\to\pm 1$, $\gamma_z\to 0$, and $\gamma_z\to\pm 1$). Efficient, accurate routines for the evaluation of P_n, P_r, and P_z are available [38]. Interestingly, the limit for $\Delta r\to 0$ leads to the continuum boundary conditions of

$$\frac{\partial f_0}{\partial r} = -\frac{2}{\lambda_M} f_0, \quad \frac{\partial f_{1r}}{\partial r} = -\frac{2}{\lambda_M} f_{1r}, \quad \frac{\partial f_{1z}}{\partial r} = -\frac{2}{\lambda_M} f_{1z}, \tag{23}$$

along with the limiting forms of the absorption terms [Eqs. (19) etc.] which will exhibit infinite absorption rates as $d=\frac{1}{2}\Delta r\to 0$.

IV. HEAVY-PARTICLE EQUATIONS

The heavy particles (neutral neon, metastable states 3S3P2 and 3S3P0, and ion) are considered to exchange energy so well among themselves and with each other that they substantially achieve a Maxwellian distribution at a common temperature. Equations for the conservation of mass and momentum are solved for each species. Since heating of the neutral gas is allowed, an energy conservation equation is solved for the neutral gas.

Beginning with the neutral gas, it must be considered that radial flow of ions to the wall will drag neutral gas, and cause a parasitic flow. This parasitic radial flow is counteracted by axial flow tending to reequilibrate the pressure. Without knowledge of the axial conditions, it is impossible to specify the rate of this reequilibration. The flow is inherently two dimensional, and thus requires some term to represent the axial flow that results from the radial flow of neutral gas. A heuristic approach is taken by introducing a time constant for pressure relaxation τ_z, to describe the equilibrating effect. For large values of τ_z, axial flow is slow, and a radial pressure difference will be maintained. For small values of τ_z, radial pressure is quickly equilibrated. The mass conservation equation for neutral gas is thus

$$\frac{\partial N}{\partial t}+\frac{1}{r}\frac{\partial(rNv_{Nr})}{\partial r}+\frac{\partial(Nv_{Nz})}{\partial z}=0, \tag{24}$$

where $N(r)$ is the neutral gas (neon) concentration, and v_{Nr} its radial velocity. The axial term is estimated as

$$\frac{\partial(Nv_{Nz})}{\partial z}\approx-\frac{N}{\tau_z}\left(1-\frac{p_N}{p_0}\right), \tag{25}$$

where $p_N(r)$ is the local gas pressure $[p_N(r)=N(r)kT(r)]$ and p_0 is the reservoir pressure.

Momentum conservation is represented by

$$\frac{\partial(Nv_{Nr})}{\partial t}+\frac{1}{r}\frac{\partial(rNv_{Nr}v_{Nr})}{\partial r}=-\frac{\partial p_N}{\partial r}+\omega_i N n_i(v_{ri}-v_{Nr}), \tag{26}$$

where v_{ri} is the radial velocity of the ion gas, and ω_i is a collision rate for momentum transfer between neutral neon and the neon ion taken from the mobility estimates [39].

Energy conservation for the neutral gas is represented by

$$\frac{\partial(Nu_N)}{\partial t}+\frac{1}{r}\frac{\partial(rNu_Nv_{Nr})}{\partial r}=\frac{1}{r}\frac{\partial}{\partial r}\left(r\kappa\frac{\partial T}{\partial r}\right)-p_N\frac{1}{r}\frac{\partial(rv_{Nr})}{\partial r}-\omega_e, \tag{27}$$

where $u_N(r)=\frac{3}{2}(k/e)T(r)$ is the neutral thermal energy, ω_e is a term representing collisional exchange of energy with electrons,

$$\omega_e(r)=\frac{e}{m}N(r)\int_0^\infty\left[u\frac{\partial}{\partial u}\left(vu\delta_{el}\sigma_{el}\frac{kT}{e}\frac{\partial\eta}{\partial u}\right)-\delta_{el}\sigma_{el}v\left(u-\frac{1}{2}\frac{kT}{e}\right)\eta\right]du, \tag{28}$$

and $\kappa(T)$ is the thermal conductivity for neon [40].

For ions, mass conservation is as follows:

$$\frac{\partial n_i}{\partial t}+\frac{1}{r}\frac{\partial(rn_iv_{ir})}{\partial r}=\Omega_i, \tag{29}$$

where the ionization rate Ω_i is determined from the electron energy distribution as

$$\Omega_i=\frac{e}{m}\sum_j N_j\int_0^\infty\eta\sigma_{i,j}v\,du, \tag{30}$$

where N_j refers to each of the ionizing species, namely, neutral neon, 3S3P0 metastable state, and 3S3P2 metastable state.

Momentum conservation for ions is

$$\frac{\partial n_iv_{ir}}{\partial t}+\frac{1}{r}\frac{\partial(rn_iv_{ir}^2)}{\partial r}=\frac{e}{M}n_iE_r-\frac{1}{M}\frac{\partial p_i}{\partial r}+\omega_in_iN(v_{Nr}-v_{ir}), \tag{31}$$

where $p_i(r)=n_i(r)kT(r)$ is the ion pressure and E_r is the radial component of electric field, $\vec{E}$.

For each of the metastable excited species, the transport equations are similar to those of the ions, but without the electric force term in the momentum equations.

Boundary conditions for the ions and metastable states are taken to be the obvious symmetry conditions at the axis ($n_i[0]=n_i[1]$; $v_{ir}[0]=-v_{ir}[1]$) and perfectly absorbing at the wall. The absorbing-wall condition is derived from the same argument that led to the absorbing-wall conditions for electrons, but for the heavy-particle consideration is made for the assumed Maxwellian distribution function. The result is a set of conditions for the ions that are similar to those for electrons, with an absorption term and a projected boundary condition. Details of this derivation can be found elsewhere [37].

V. FIELD EQUATIONS

Poisson's equation can also be written in time-dependent form. The need for such a form comes from the tendency of a static representation of Poisson's equation to exhibit numerical instability in a time-dependent simulation due to the infinitely fast propagation of roundoff error that creates a violation of the Courant stability criterion.

A fictitious electric field "velocity" $V_E(r)$, is used to multiply Poisson's equation ($\vec{\nabla}\cdot\vec{E}=\rho_c/\epsilon_o$):

$$\vec{\nabla}\cdot(\vec{E}V_E)=\frac{1}{\epsilon_o}\rho_cV_E+\vec{E}\cdot\vec{\nabla}V_E, \tag{32}$$

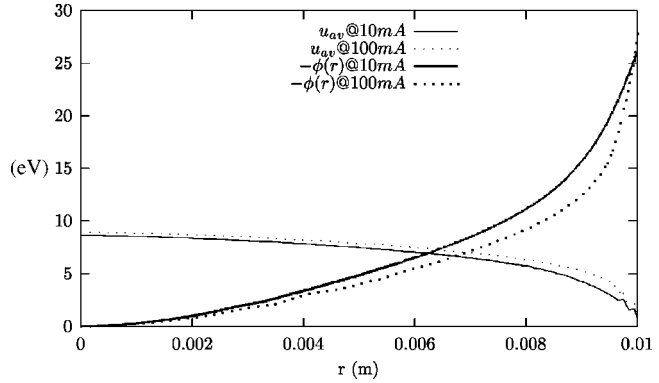

FIG. 1. Average electron energy and radial potential as a function of radial position for 10-mA and 100-mA steady-state currents at $R=1$ cm in neon at 1 Torr.

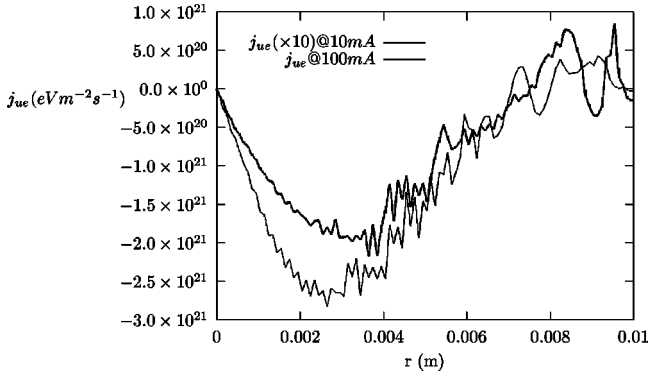

FIG. 2. Radial electron energy flux as a function of radial position for 10-mA and 100-mA steady-state currents at $R=1$ cm in neon at 1 Torr.

which, when added to the magnetostatic form of Ampere's law $[(\partial\vec{E}/\partial t)+(1/\epsilon_o)\vec{J}=0]$, gives another dynamic equation for E_r. In cylindrical coordinates with axial uniformity, this is

$$\frac{\partial E_r}{\partial t}+\frac{1}{r}\frac{\partial(rE_rV_E)}{\partial r}=\frac{e}{\epsilon_o}(\Gamma_{er}-n_iv_i)+E_r\frac{\partial V_E}{\partial r}+\frac{1}{\epsilon_o}(n_iq_i-en_e)V_E, \tag{33}$$

where Γ_{er} is the radial electron flux. Equation (33) is a convective flow equation, with some unusual source terms. V_E can take on many possible forms. It has been found that a very simple form works well:

$$V_E(r)=V_x\frac{r^2}{R^2}, \tag{34}$$

where the constant V_x is chosen for accuracy. The choice should be small enough to ensure that Eq. (33) does not limit the time step (via the Courant condition) of the simulation, while at the same time guaranteeing that the static Poisson's equation is well represented in, and does not disappear into the roundoff error of, the dynamic equation. A value of V_x chosen to be the about 1% of the electron speed of the maximum electron energy has been found to work well. It can also be shown (see details in Ref. [41]) that the system of equations is dynamically stable only for $V_x>0$.

Finally, the axial field is calculated by inserting the discharge into a circuit with a current source of magnitude I_o and a parallel capacitance C_l, chosen to be so sufficiently small that it does not dominate the rate of relaxation to steady state, nor allow a relaxation oscillation to occur. A value of 300 pF m is used in these simulations in neon. This technique eliminates the difficulty of enforcing a constant condition on the axial current. Instead, the axial current is calculated from

$$I=-2\pi e\int_0^R\Gamma_{ez}r\,dr=-2\pi e\frac{e}{m}\int_0^R\int_0^\infty X_z\eta v\,du\,r\,dr, \tag{35}$$

and the axial field is determined from the time-dependent equation

$$\frac{dE_z}{dt}=\frac{1}{C_l}(I_o-I). \tag{36}$$

VI. RESULTS

The complete set of time-dependent equations for electron, ion, metastable, and neutral species, along with both radial and axial electric field have been solved numerically for a particular sequence of conditions. A grid is chosen with 50 uniformly spaced cells in radial position, and 100 nonuniformly (higher density at lower values) spaced cells in kinetic energy. Beginning with some arbitrary initial condition (chosen as a Maxwellian distribution for electrons in this case) the computation proceeds with $I_o=100$ mA until steady state is reached. A change is then made to $I_o=10$ mA and computation proceeds until steady state is again reached. The steady-state results are then remapped

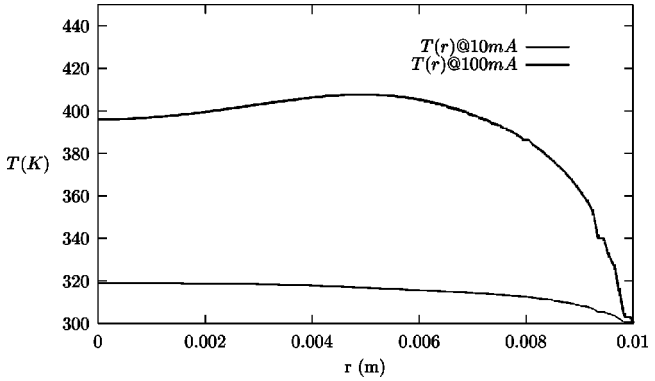

FIG. 3. Radial neutral gas temperature profiles at two values of steady-state current. Although the complete thermal steady state has not been completely reached for either case, there is clearly a different trend caused by parasitic flow at the higher current.

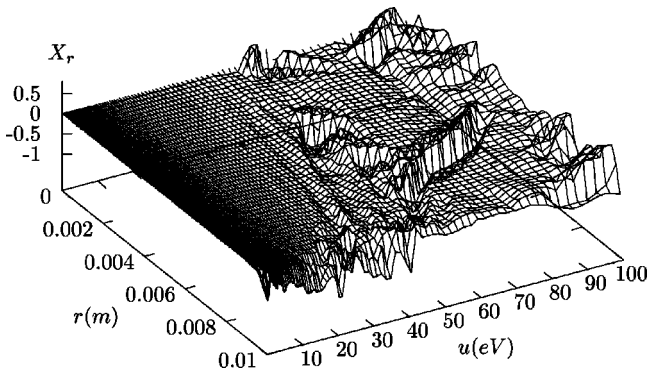

FIG. 4. Radial anisotropy as a function of energy and position, at 10 mA. The natural boundary of trapped electrons is clearly visible, which mirrors the potential profile.

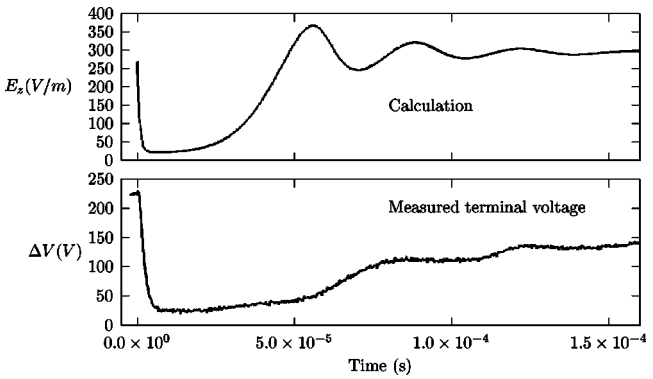

FIG. 5. Transient response of axial field (calculated) and terminal voltage (measured) to step change in current.

onto a grid with 100 radial cells and 200 energy cells and run for 1 μsec to get higher resolution and to test the truncation error.

The entire distribution function is available for all of these conditions, although it is often most convenient to plot only certain derived moments of these. For example, Fig. 1 shows the average electron energy as a function of radial position for both steady-state values of current.

Another important moment quantity is the radial heat flux j_{ue}, defined as

$$j_{ue}(r) = \int_0^\infty u f(r,u) v_r \, d^3v = \frac{e}{m} \int_0^\infty u X_r \eta v \, du \qquad (37)$$

and shown in Fig. 2. It is clear that the significant negative excursion of this quantity, as first described for an energy-resolved kinetic description by Uhrlandt and Winkler [4] (and later confirmed by others [1,15]) is also found by the present techniques.

One interesting aspect of the present simulation is the description of neutral gas heating. The model described above relies on an axial relaxation parameter τ_z to determine the degree of pressure equilibration allowed in response to the parasitic radial gas flow caused by radial ion flow. For the chosen τ_z of 100 ns, the effects on heavy-particle temperature is shown in Fig. 3. While it could be argued that the thermal time constant of the system is somewhat longer than the 100–150 μs of the simulation time, and that true steady state is not yet established, there is clearly a different trend for the two current levels. At the higher current, the parasitic flow is such that convection cools the central regions (subject to the model assumptions), while carrying heat and compressively heating the outer regions. At the lower current, the parasitic flow is much lower, and a more conventional profile is obtained.

The radial anisotropy X_r for the 10-mA steady state is shown in Fig. 4. From this it is clear that there is very low anisotropy within the artificial boundary of ''trapped'' electrons defined by the potential profile as shown in Fig. 1. These electrons lack sufficient energy to escape, and so spend a lot of time in this region suffering many directional changes due to collisions and electric forces. Those that manage to be taken above this boundary appear to take on a chaotic behavior at the higher energies. Upon closer examination on a short ($\approx$1ns) time scale, it becomes clear that there are waves and oscillations taking electrons out to the walls in a very dynamic process, and that steady state apparently does not strictly exist. Due to the nonlinear nature of the set of coupled equations, the presence of such unstable behavior can be important since the resulting solution will have different mean values than would a corresponding solution to the time-averaged steady-state equations. The ability to examine these unstable effects is a significant advantage of the time-dependent approach.

Complete sets of data for these conditions are available in tabular form elsewhere [42].

There is generally a lack of published measurements that can be used for verification of these results. The quantity that can be measured most easily is the axial electric field E_z. At a pressure of 1 Torr and a radius of 1 cm, there are few published measurements, most are quite old, and results are varying [43–45]. For the present work, axial field measurements were made using commonly available laboratory equipment, by means of two independent techniques. One technique utilizes short pulses of direct current, while the other utilizes a superimposed high-frequency signal. Details are given in Ref. [46]. The measurements are performed on custom-made neon tubes obtained from a speciality lighting shop [47], made of standard *T*-25 tubing, and containing cold cathodes of the type typically found in the neon sign industry. Comparison of calculated field with these various mea-

TABLE I. Axial field calculations (in units of V/m) compared with various measurements.

	Calculated	dc [46]	ac [46]	Kagan *et al.* [45]	Lompe and co-workers [43,44]
10 mA	300	393	467	200	
100 mA	266	349	303	170	244

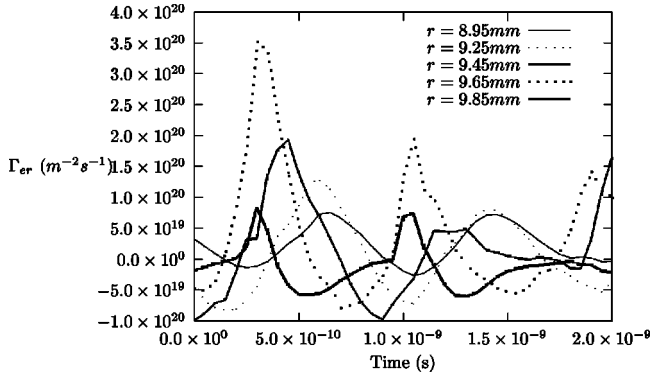

FIG. 6. Radial electron flux near the wall as a function of time for ''steady-state'' results at 100 mA. An instability is found with a time scale of 1 ns.

surements is shown in Table I. The calculated results are in reasonable agreement with experimental results that themselves vary over quite a large range.

The transient response of the terminal voltage for a step change in current from 100 mA to 10 mA is shown in Fig. 5. It is clear that the initial response (on a time scale of a few μs) to the step is largely ohmic, and that quite some time is needed in order to reestablish the ionization balance. In the subsequent steady state (several hundred μs later), after ionization balance has been reestablished, the nonohmic result is such that the voltage at the lower current is somewhat higher than that at the higher current. The figure also shows the calculated values of axial field for the transient connecting the two steady states. From this comparison it can be seen that the calculated transient response of the positive column generally resembles the measured response of terminal voltage, although with a somewhat faster recovery. Since the terminal voltage measurement includes all transient effects associated with anode and cathode processes, as well as all axial effects that are only crudely approximated in the model, the agreement is reasonable.

VII. DISCUSSION

Due to the large disparity in relevant time scales, simulations using the described techniques are very time consuming. Typically, complete runs take 6–8 months of CPU time on a reasonably fast work station (533-MHz Alpha). Faster machines now available will reduce this time by a factor of 3–6, and another similar factor could be obtained by simply ignoring neutral gas heating with its long time constant and relatively minor contribution. However, the use of these methods is generally restricted to special test cases for which detailed information about all of the included physical effects, as well as their dynamic behavior, is needed.

The dynamic equations, together with the self-consistent boundary conditions, form an *ab initio* description of the positive column, constrained only by the assumptions of axial symmetry and axial uniformity. The only input to the model is kinetic (collisional) data, host gas pressure, and axial current. Since the model is not cast as an eigenvalue problem, there are no extraneous parameters to be adjusted in order to obtain ionization balance.

The unstable fluctuations discussed in the preceding section are particularly strong near the wall where electrons encounter a repulsive sheath. Figure 6 shows the radial electron flux on a short time scale after the steady state of 100 mA has been reached. This figure clearly shows erratic fluctuations in flux, which are large, confined to the region near the wall, very fast, and hence, do not appear in other quantities such as the computed axial field. In light of the fact that the computational time step for these computations is of the order of 1 ps, while the oscillation period is around 1 ns, and that the oscillation persists at different grid spacing and time steps, it is not likely that this effect is a numerical artifact.

To analyze this situation, it is possible to perform a linear stability analysis of the equations describing the electron gas near the wall by making some simplifying assumptions. The complete Boltzmann equation, or even the elliptic representation of it, is too unwieldy to provide a concise result. For the purposes of this stability analysis, the traditional approach of assuming a Maxwellian distribution for the electrons will be taken. The only quantities that are allowed to change on the short time scale of interest are electron concentration n_e, radial electron flux Γ_{er}, electron temperature T_e, and radial electric field E_r. The short time scale dynamics is described by the following set of equations:

$$\frac{\partial n_e}{\partial t}+\frac{\partial \Gamma_{er}}{\partial x}=0, \tag{38}$$

$$\frac{\partial \Gamma_{er}}{\partial t}+\frac{\partial \Gamma_{er} v_e}{\partial x}=-\frac{e}{m}n_e E_r-\frac{kT_e}{m}\frac{\partial n_e}{\partial x}-\nu_M \Gamma_{er}, \tag{39}$$

$$n_e\frac{\partial \frac{3}{2}kT_e}{\partial t}+n_e\frac{\partial \frac{3}{2}kT_e v_e}{\partial x}=n_e\kappa\frac{\partial^2 T_e}{\partial x^2}-\omega_e-n_e kT_e\frac{\partial v_e}{\partial x}-e\Gamma_{er}E_r, \tag{40}$$

$$\frac{\partial E_r}{\partial x}=\frac{e}{\epsilon_o}(n_i-n_e), \tag{41}$$

where ionization is considered to be too slow for a process to have an effect on the time scale of interest. Thermal conductivity κ is estimated (see Raizer [39]) as

$$\frac{\kappa}{k}=\frac{\frac{5}{2}kT_e}{\nu_M m}, \tag{42}$$

and a constant cross section of 1.9×10^{-20} m^2 is assumed for determination of the collision frequency ν_M. Linearization of these equation, and the introduction of perturbation quantities $(\tilde{n}_e,\tilde{\Gamma}_{er},\tilde{T}_e,\tilde{E}_r)$ leads to the following eigenvalue problem:

$$\alpha\tilde{n}_e+j\beta\tilde{\Gamma}_{er}=0, \tag{43}$$

$$\alpha\tilde{\Gamma}_{er}+\frac{e}{m}n_e\tilde{E}_r+\frac{e}{m}E_r\tilde{n}_e+j\beta\frac{kT_e}{m}\tilde{n}_e+\nu_M\tilde{\Gamma}_{er}=0, \tag{44}$$

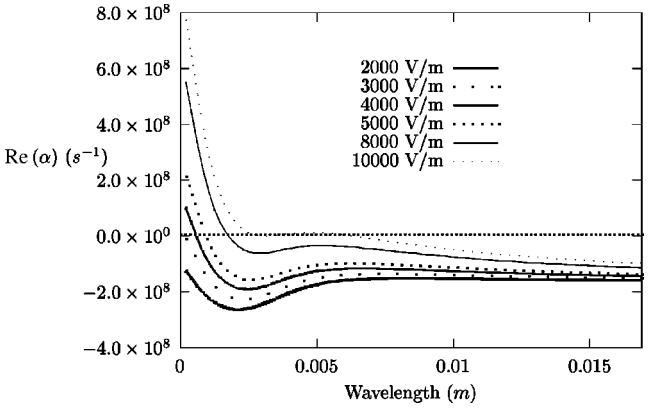

FIG. 7. Results of eigenvalue analysis of a simplified short time scale stability model. The real part of the eigenvalue, Re(α), is shown as a function of wavelength. Instability is indicated by positive values of Re(α). The associated oscillatory frequency for the unstable portions, found from the imaginary part of α (not shown), is of the order of 1×10^{9} s^{-1}.

$$\alpha n_e k\tilde{T}_e + j\beta\frac{5}{2}(\tilde{\Gamma}_{er} - v_e\tilde{n}_e) + j\beta v_e\frac{3}{2}n_e k\tilde{T}_e + \frac{\kappa}{k}\beta^2 k n_e k\tilde{T}_e + e\Gamma_{er}\tilde{E}_r + eE_r\tilde{\Gamma}_{er} = 0, \tag{45}$$

$$j\beta\tilde{E}_r = -\frac{e}{m}\tilde{n}_e, \tag{46}$$

where α is the (complex) temporal growth parameter and β is the (real) spatial wave number of the perturbation with wavelength λ ($\beta=2\pi/\lambda$). For conditions found near the wall, as determined by the results of the detailed computation, the eigenvalues of this system are found by Schur decomposition [48]. The result of this analysis for a wide range of wavelengths and radial fields is shown in Fig. 7. Clearly, for sufficiently short wavelengths, there are eigenvalues with positive real part, indicating physical instability. Furthermore, the imaginary part of those eigenvalues indicate that the temporal frequencies of the resulting unstable modes are of the order of 10^{9}s^{-1}. This result is quite comparable with the time scale found by the detailed time-dependent calculation of the present work (see Fig. 6), suggesting that the instability is not an artifact of the solution, but a feature of the transport equations and, hence, has a physical basis.

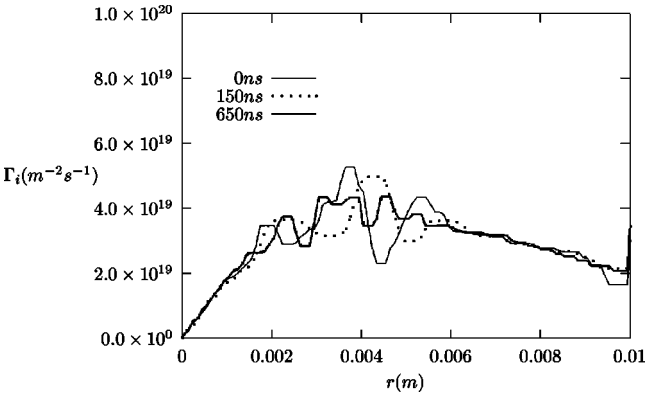

FIG. 8. Computed results of radial ion flux at several points in time for $I=100$ mA. The long-wavelength, low-frequency oscillation near $r=0.5$ cm is apparent.

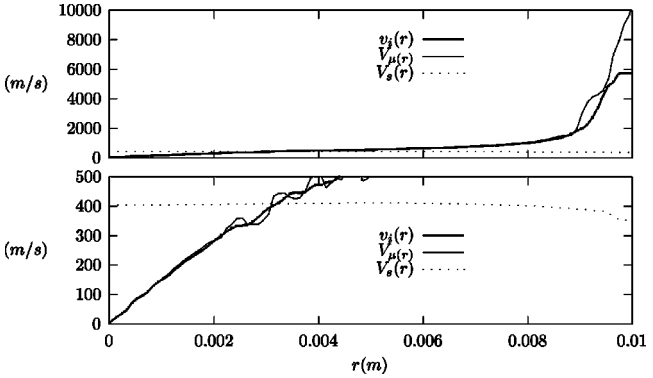

FIG. 9. Computed results of radial ion velocity shown along with local sonic speed $V_s=\sqrt{kT(r)/M}$ and mobility limited speed $V_\mu=\mu_i E_r$ for $I=100$ mA.

A fluctuation also appears in the ion flux, as shown in Fig. 8 for several disparate points in time near the steady state at 100 mA. No attempt has been made here to analyze the stability of this region on the appropriate time scale, however, its location appears to coincide with the region in which the radial ion velocity crosses through the ion sonic speed. When an average is taken over several μs in order to filter that fluctuation, the ion velocity profile shown in Fig. 9 is obtained. This figure confirms the analytical result of Ingold [14] in which the ion velocity crosses the ion sound speed at roughly the same point as the ion mobility speed (defined as $\mu_i E_r$) also crosses the sonic speed. In fact, from the present result, it would appear that the ion velocity is nearly identical to the mobility speed everywhere except near the wall, and that the ion pressure term can, for all practical purposes, be neglected, despite the inclusion of a finite ion temperature.

Due to the high degree of stiffness in this system, the radial fluxes, derived from moments of f_{1r} (or X_r), exhibit a much greater sensitivity to small fluctuations in conditions than do the quantities derived from moments of f_0 (or η). Figure 10 shows electron and ion concentration profiles for currents of both 10mA and 100mA, from which it is seen

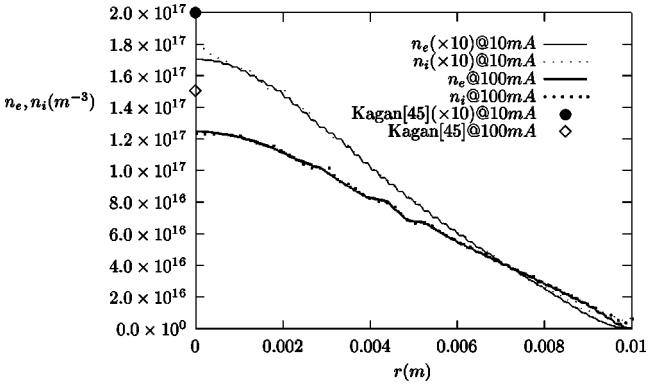

FIG. 10. Computed charged particle concentration profiles at both steady-state currents of 10mA and 100mA. Also shown are measurements of Kagan *et al.* [45].

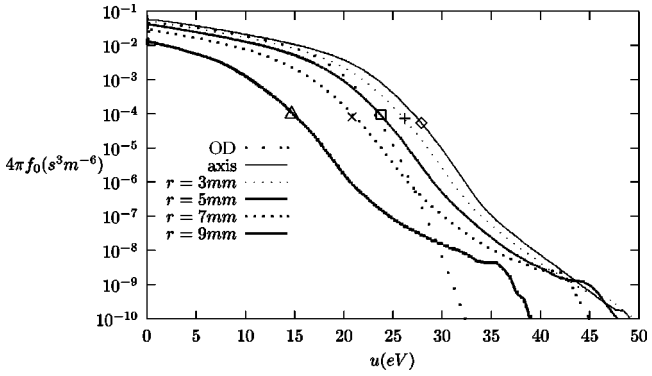

FIG. 11. Isotropic component of EVDF, $4\pi f_0(r,u)$, at 100 mA, at selected radii. Symbols ($\diamond,\square,\times,\triangle$) indicate the value of $\phi(r)-\phi_W$ corresponding to the boundary between trapped and untrapped electrons at that radius. Also shown is the zero-dimensional solution for on-axis conditions.

that the profiles are quite smooth, and that quasineutrality holds nearly everywhere, except at the wall. The fluctuations in radial fluxes are evidently small enough and fast enough to not disrupt these quantities. These results compare very favorably with the measurements of Kagan *et al.* [45].

Although these computational techniques are applicable at higher pressures as well, the presented results pertain to pressures such that nonlocal conditions exist. Nonlocal effects [16] tend to cause f_0 to be nearly a function of total energy (kinetic plus potential). This trend is somewhat confirmed by Fig. 11, in which the isotropic component of the EVDF is shown at various radii. Each curve is roughly the same as the on-axis curve, shifted in energy by the local potential $\phi(r)$. Trapped on-axis electrons have energies below the wall potential of 27 V. The excitation processes with energies at about 16.6 eV have a marked effect on f_0, and cause a precipitous decline above that energy. The off-axis curves then mirror this decline, although without a corresponding decline in the actual excitation energy. Thus, off axis, the axial field serves to replenish these artificially depleted energies, such that a repletion of tail electrons exists over and above what would exist had the on-axis distribution simply shifted according to the local potential. Due to this ''inversion,'' tail electrons can then return to the axis along a different, higher total energy path than what brought them outward. This effect has already been evidenced by the presence of a negative heat flux (Fig. 2), while the particle flux (a lower moment,

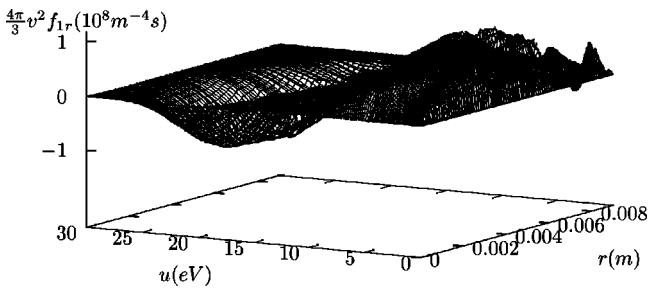

FIG. 12. Computed radial component of EVDF, $(4\pi/3)v^2 f_{1r}(u,r)$, at 100 mA.

shown in Fig. 9) remains positive. f_{1r} clearly must swing from positive at low energies to negative at higher energies in order to give that result. Figure 12 shows this bimodal characteristic at 100 mA. Trapped electrons are, in general, flowing in a loop in phase space in which they move outward at lower energies, upward in energy as their radial motion slows, and inward at higher energies. The axial field adds energy to the low-energy electrons so as to maintain their ascent up the space charge potential and, at some point, to move these to higher energies where their net motion will be inward. There is a significant energy change along this loop, bringing into question the assertion often made [17,18] that total energy is a ''constant of the motion'' of these trapped electrons.

With such a concern, it remains to be determined just *how nearly* a function of total energy f_0 is, and what use can be made of this property. When applied to the present cylindrical geometry, the original work of Bernstein and Holstein [18] would lead to taking $f_{1r}=0$, for a first approximation, according to the two-term expansion relation

$$f_{1r}=-\lambda_M\left(\frac{\partial f_0}{\partial r}-E_r\frac{\partial f_0}{\partial u}\right), \tag{47}$$

when $f_0=f_0[u-\phi(r)]$. Neglect of f_{1r} in the next relation of the spherical harmonic expansion

$$\frac{u}{3}\frac{1}{r}\frac{\partial(rf_{1r})}{\partial r}-\frac{\partial}{\partial u}\left(\frac{1}{3}u(E_rf_{1r}+E_zf_{1z})-\delta_{el}u^2\frac{1}{\lambda_M}f_0\right)=S_{inel} \tag{48}$$

leads directly to the integration described, for example, in Eq. (40) of Ref. [18] as a first approximation for f_0.

Equation (48) can be viewed as the divergence of fluxes of a flow in phase space. However, under nonlocal conditions, the elastic collision term of Eq. (48) is relatively small and, considering circulation in phase space described above, it is clear that neglect of f_{1r} in Eq. (48) is tantamount to neglect of a quantity comparable to those retained. It is exactly the conservation in phase space, as described by Eq. (48), which determines that the contribution of f_{1r} is *not* negligible. Although its magnitude will be much smaller than f_{1z}, its extra weighting by E_r makes its contribution significant. Furthermore, both the weighting (by E_r) and the magnitude of f_{1r} in comparison with increasing f_{1z} increase with radius, so that the relative contribution of these neglected terms grows with radial position.

In order to show the effects of nonlocality, the curve of Fig. 11 labeled ''0D'' is shown, which is the result of a zero-dimensional Boltzmann solution for the conditions present on axis ($E_z=266$ V/m, $N=2.41\times10^{22}$ m^{-3}, $n_{3s3P0}=1.75\times10^{17}$ m^{-3}, $n_{3s3P2}=6.2\times10^{17}$ m^{-3}). A much greater depletion of the energies above threshold is found than in the corresponding complete solution. Evidently the inflow of electrons into this region from radial positions with higher potential energy is very significant.

Accordingly, the first approximation of the nonlocal electron kinetic approach analyzed in Sec. II is equivalent to solving a similar (albeit, spatially averaged) zero-

dimensional Boltzmann equation for the on-axis conditions, and then translating this solution to other positions by shifting the energy axis according to the local potential. That the surplus of electrons above the ''translated'' threshold grows with radius, as evidenced by the inward radial heat flux, is further indication that the NEK approximation becomes worse with increasing radius. Uhrlandt and Winkler [4] reached a similar conclusion, and also indicate that the assumed strict dependence of f_0 on total energy also leads, even without spatial averaging, to the neglect of a radial flux term. In fact, in somewhat a self-contradictory manner, the NEK method [see, for example, Ref. 5 Eq. (7) using Eq. (18) at $r=0$, compared with Eq. (19)] could also be solved on axis to yield exactly a zero-dimensional solution. Although the concept of f_0 as nearly a function of total energy is perhaps useful for qualitative analysis, the NEK methodology for determining f_0 does not properly describe the circulation of electrons in phase space, and hence does not correctly represent the physics of energy flow and electron reuse in the column.

Quantitatively, the detailed computation finds a value for the ratio $|f_{1z}/f_0|$ of about 0.06 near the axis at low energies. The ratio (f_{1r}/f_0) changes with radius, and grows to a maximum roughly where the subexcitation on-axis electrons reach their (radial) turning point, near $r=8$ mm. There, $(f_{1r}/f_0)\approx 0.006$, which, although smaller than $|f_{1z}/f_0|$, is not negligible when each is weighted by their respective field components ($E_r \gg E_z$ at $r=8$ mm).

In the nonlocal regime, the energy balance is established via the radial circulation effect described above and eventually culminates in inelastic events near the axis. For this reason, a simple estimate for the ratio $|f_{1z}/f_0|$ in terms of fundamental quantities in the nonlocal regime is not obvious. In contrast, energy loss in the local regime is dominated by elastic collisions, leading to the familiar estimate of $|f_{1z}/f_0|\approx\sqrt{\delta_{el}}$ [49].

VIII. SUMMARY

A time-dependent, nonstatistical, first-principles description of the dc positive column at low pressure has been presented, analyzed, and compared with both static and dynamic measurements of axial electric field in low-pressure neon under nonlocal conditions. The very versatile technique for generating these continuum solutions is equally applicable at higher pressures. The elliptic representation of the Boltzmann equation has been reformulated in a manner that has numerical advantages. A self-consistent absorbing-wall boundary condition for the continuum equations has been devised, implemented, and described in detail. A time-dependent form of Poisson's equation has been derived and implemented. In addition to a detailed static picture of the state of the discharge, a dynamic description is also generated. The temporal evolution of the positive column is thus quantitatively described as it responds to changes in conditions, or as those conditions potentially lead to physical instability. The technique should lend itself to such situations as afterglows in which time-dependent solutions are necessary.

Under nonlocal conditions, the utility of the concept of the EVDF being nearly a function of total energy is seen to be quite valid for its isotropic component, but to be of little utility in actually determining that EVDF. In agreement with Uhrlandt and Winkler [50], the present work indicates that the problem remains the one for which a detailed computation is required.

ACKNOWLEDGMENT

The author would like to thank John Ingold for countless valuable discussions of the positive column and the history of its analysis.

[1] U. Kortshagen and J.E. Lawler, J. Phys. D **32**, 2737 (1999).
[2] G.J. Parker and W.N.G. Hitchon, Jpn. J. Appl. Phys., Part 1 **36**, 4799 (1997).
[3] L.L. Alves, G. Gousset, and C.M. Ferreira, Phys. Rev. E **55**, 890 (1997).
[4] D. Uhrlandt and R. Winkler, J. Phys. D **29**, 115 (1996).
[5] C. Busch and U. Kortshagen, Phys. Rev. E **51**, 280 (1995).
[6] E.A. Richley, Phys. Rev. E **59**, 4533 (1999).
[7] J.P. Gassiot, Proc. R. Soc. Edinb [Biol] **IX**, 601 (1858).
[8] M. Plucker, Philos. Mag. **16**, (1858).
[9] J.P. Gassiot, Proc. R. Soc. Edinb [Biol] **X**, 432 (1860).
[10] W. Schottky, Phys. Z. **XXV**, 635 (1924).
[11] L. Tonks and I. Langmuir, Phys. Rev. **34**, 876 (1929).
[12] W.P. Allis and D.J. Rose, Phys. Rev. **93**, 84 (1954).
[13] J.R. Forrest and R.N. Franklin, J. Phys. A **1**, 1357 (1968).
[14] J.H. Ingold, Phys. Fluids **15**, 75 (1972).
[15] J.H. Ingold, Phys. Rev. E **56**, 5932 (1997).
[16] L.D. Tsendin, Sov. Phys. JETP **39**, 805 (1974).
[17] L.D. Tsendin, Plasma Sources Sci. Technol., 200 (1995).
[18] I.B. Bernsteinand and T. Holstein, Phys. Rev. **94**, 1475 (1954).
[19] E.A. Richley, see http://www.onion-switch.com/physics/poscol/nek.pdf
[20] E.A. Richley, see http://www.onion-switch.com/physics/poscol/nek.c.
[21] U. Kortshagen, G.J. Parker, and J.E. Lawler, Phys. Rev. E **54**, 6746 (1996).
[22] G.J. Parker, W.N.G. Hitchon, and J.E. Lawler, Phys. Rev. E **50**, 3210 (1994).
[23] E.S. Oran and J.P. Boris, *Numerical Simulation of Reactive Flow* (Elsevier, New York, 1987).
[24] W.G. Vincenti and J. Charles H. Kruger, *Introduction to Physical Gas Dynamics* (Krieger, 1977).
[25] S.T. Zalesak, J. Comput. Phys. **31**, 335 (1979).
[26] L.F. Shampine, *Numerical Solution of Ordinary Differential Equations* (Chapman and Hall, London, 1994).
[27] K. Valentini, J. Phys. D **21**, 311 (1988).
[28] D.L. Book, J.P. Boris, M.A. Fry, R.H. Guirguis, and A.L. Kuhl, Naval Research Laboratories Memorandum Report No. 4914, 1982 (unpublished).

[29] A.G. Robertson, J. Phys. B **5**, 648 (1972).
[30] H.S.W. Massey and E.H.S. Burhop, *Electronic and Ionic Impact Phenomena* (Clarendon, Oxford, 1952).
[31] D.F. Register and S. Trajmar, Phys. Rev. A **29**, 1785 (1984).
[32] D.F. Register, S. Trajmar, G. Steffensen, and D. Cartwright, Phys. Rev. A **29**, 1793 (1984).
[33] H. Margenau, Phys. Rev. **73**, 297 (1948).
[34] M. Johnston, K. Fujii, J. Nickel, and S. Trajmar, J. Phys. B **29**, 531 (1996).
[35] D. Rapp and P. Englander-Golden, J. Chem. Phys. **43**, 1464 (1965).
[36] P. Morse and H. Feshbach, *Methods of Mathematical Physics* (McGraw-Hill, New York, 1953).
[37] E.A. Richley, see http://www.onion-switch.com/physics/poscol/WallConditions.ps
[38] E.A. Richley, see http://www.onion-switch.com/physics/poscol/WallRoutines.html
[39] Y.P. Raizer, *Gas Discharge Physics* (Springer-Verlag, Berlin, 1991).
[40] S. Chapman and T.G. Cowling, *The Mathematical Theory of Non-Uniform Gases* (Cambridge University Press, Cambridge, England, 1990).
[41] E.A. Richley, see http://www.onion-switch.com/physics/poscol/WallStability.ps
[42] E.A. Richley, see http://www.onion-switch.com/physics/poscol_results/
[43] V.A. Lompe and R. Seeliger, Ann. Phys. (Paris) **15**, (1932).
[44] A.V. Engel and M. Steenbeck, *Elektrische Gasentladungen ihre Physik und Technik* (Springer-Verlag, Berlin, 1934).
[45] Y.M. Kagan, R.I. Lyagushchenko, and A.D. Khakhaev, Opt. Spektrosk. **14**, 598 (1963) [Opt. Spectrosc. **14**, 317 (1963)].
[46] E.A. Richley, see http://www.onion-switch.com/physics/poscol/experiment.ps
[47] Cathode Lighting Systems, Inc., Gaithersburg, MD, http://www.cathodelightingsystems.com
[48] D.E. Stewart and Z. Leyk, http://www. netlib.org/c/meschach
[49] K.-U. Riemann, Phys. Rev. A **46**, 4717 (1992).
[50] D. Uhrlandt and R. Winkler, Plasma Chem. Plasma Process. **16**, 517 (1996).